Atomic structure of dislocation cores in GaN

Antoine Béré and Anna Serra*
Departament de Matemàtica Aplicada III, Universitat Politècnica de Catalunya, Jordi Girona 1-3, 08034 Barcelona, Spain
(Received 9 October 2001; revised manuscript received 24 January 2002; published 20 May 2002)

The atomic structures of **a** and **c** dislocation cores in the wurtzite gallium nitride have been studied by atomic computer simulation using an interatomic potential of the Stillinger-Weber type. Initially, the field of displacements is imposed according to the classical linear elasticity theory and then the system is relaxed to the minimum energy. The dislocation cores present multiple structures that can be related to the location of the dislocation line. The shape and extension of the dislocation cores are analyzed by means of the atomic relative displacements map. The core energy E_c and core radius r_c are determined by fitting the strain energy stored in the cylinder of radius R, centered on the dislocation line, to the expression $E_s(R)=A_0\ln(R/r_c)+E_c$.

DOI: 10.1103/PhysRevB.65.205323 PACS number(s): 61.72.Lk, 71.15.Nc, 71.55.Eq, 61.72.Bb

I. INTRODUCTION

GaN is a semiconductor that presents a high applicability in optoelectronics and in high-power, high-frequency devices. The defects lying on the surface of the substrate and/or the difference in lattice parameters and thermal expansion coefficients between the GaN and the substrate induces in the grown GaN a high density of threading dislocations. Moreover, if the growth process is nucleated in islands, tilt boundaries are created that can be explained in terms of sequences of edge dislocations.[1,2] Thus, provided most of crystallite imperfections (impurities, vacancy, dislocations, and grain boundaries) can give rise to electronic states throughout the band gap, it is important to know their atomic structure from which an understanding of the optical properties can be developed. In this paper we present the core structures of edge and screw dislocations in GaN studied by atomic computer simulation using a modified Stillinger-Weber (SW) empirical potential. The same potential has been used in the study of [0001] tilt boundaries.[1]

II. EXPERIMENTAL EVIDENCE

The nature of the dislocations existing in good-quality GaN is currently well identified. Three types of threading dislocations are observed in epilayers grown on the substrate (0001) plane with Burgers vectors $\frac{1}{3}\langle 1\bar{2}10\rangle$ (*a* type of edge character), [0001] (*c* type of screw character), and $\frac{1}{3}\langle 11\bar{2}3\rangle$ ($a+c$ type of mixed character). It has been found that, under certain techniques of growth, such as the two-step epitaxial lateral overgrowth (2S-ELO) process,[3] the dislocation line changes its orientation from [0001] to a direction lying on the basal plane. Thus, there is evidence of the creation of *c*-type dislocation with edge character and *a*-type dislocation with screw character during the growth process. The atomic structure of the core of prism edge dislocations has been investigated by high-resolution electron microscopy (HREM) (Ref. 2) and by *Z* contrast[4] and three different cores have been identified, named the 4, 8, and $\frac{5}{7}$ atom rings. In[4–6] *c*-type dislocation with screw character are reported. These dislocations can have either a full core or an open core. The later are described as nanopipes of hexagonal section that terminate on the free surface of the film.

III. COMPUTER MODELING

A. Computational method

The system was created initially as a perfect crystal in the form of a rectangular parallelepiped with sides along the $[1\bar{2}10]$, $[10\bar{1}0]$, and [0001] directions. Periodic boundary conditions were applied along the dislocation line direction and fixed boundaries were imposed along the other two perpendicular directions. The outer region that forms the fixed boundaries has a thickness such that all inner region atoms have a full neighborhood within the range of the interatomic potential. Each dislocation was introduced by imposing the displacements of the isotropic linear elasticity theory[7] on the inner and outer region atoms. Since the dislocation core may present more than one stable configuration depending on the location of the origin of displacements,[8] a systematic study of the possible cores has been done by changing the position of the dislocation line. We notice that only the positions that led to nonidentical configurations are reported here and presented in Figs. 3–5, 8, 10, 11, and 14.

For the prism edge and **c** screw dislocations with dislocation line along the [0001] direction, the size of the parallelepiped was $60\ a_0\ [1\bar{2}10]\times 60\sqrt{3}/2\ a_0\ [10\bar{1}0]\times 2\ c_0\ [0001]$ with a total of 28 800 atoms. For the basal screw and **c** edge dislocations that have their dislocation line along the $[1\bar{2}10]$ direction, the crystal size considered was $60\sqrt{\frac{3}{2}}\ a_0\ [10\bar{1}0]\times 30\ c_0\ [0001]\times 4\ a_0\ [1\bar{2}10]$ with a total of 28 800 atoms (a_0 and c_0 are the equilibrium lattice parameters).

The calculation of the configuration of minimum energy is performed using the so-called quench molecular dynamics method.[9] The system is divided into two coaxial cylindrical regions (inner relaxable region and outer fixed boundary) with the axis along the dislocation line and radii $14.4a_0$ (46 Å) and $18.4a_0$ (59 Å). A thermodynamic temperature is calculated at each step and the relaxation finish when this temperature is less than 10^{-6} K.

B. Interatomic potential

Nandedkar and Narayan[10–11] have studied the atomic structure of dislocations in Si, Ge, and diamond using four empirical potentials, namely, the Baraff, Keating, Stillinger-

TABLE I. Parameters for the Stillinger-Weber potential and calculated structural properties of wurtzite structure. Experimental values are between parentheses.

	Aïchoune *et al.* (Ref. 14)			Present work		
	Ga-N	Ga-Ga	N-N	Ga-N	Ga-Ga	N-N
	Parameters of the Stillinger-Weber potential					
ε (eV/bond)	2.17	0.655	0.655	2.17	1.2	1.2
σ (Å)	1.695	2.038	1.302	1.695	2.1	1.3
λ	32.5	26.76	26.76	32.5	32.5	32.5
$a(r_c/\sigma)$	1.8	1.8	1.8	1.8	1.6	1.8
A	7.917	7.917	7.917	7.917	7.917	7.917
B	0.720	0.720	0.720	0.720	0.720	0.720
	Lattice parameters					
a (Å)	3.23 (3.19)[a]					3.19 (3.19)[a]
c (Å)	5.28 (5.18)[a]					5.20 (5.18)[a]
	Inversion domain boundaries excess energies ΔE					
ΔE (mJ/m^2)	IDB		Not stable			2590 (2663)[b]
	IDB*		702 (400)[b]			949 (400)[b]

[a]Experimental data.
[b]Ref. 16.

Weber (SW), and Tersoff potentials. They report that the SW and Tersoff potentials describe the dislocation atomic structure better. In the framework of the SW potential for Si (Ref. 12) a series of potentials have been adapted to the study of III-V semiconductors.[13] Recently, the radial (two body) and angular (three body) terms describing the energy of a GaN system have been derived by Aichoune and co-workers[14] that take into account the specificity of the different bonds, namely, Ga-N, Ga-Ga, and N-N. The fitting parameters were the lattice parameters, experimental elastic constants and the results of the *ab initio* calculations for an inversion domain boundary (IDB, described by the Holt model[15]) performed by Northrup and co-workers.[16] In fact, these authors claim that the IDB structure is quite unstable in GaN, and would relax to another inversion domain boundary named IDB* having no wrong bonds. This structure can be formed by translating one side of an IDB by $c/2$ along the [0001] direction. Nevertheless, Potin and co-workers[17] reported an experimental evidence of the existence of both inversion domain boundaries. The parameters given by Aichoune and co-workers[14] are such that they only stabilizes the IDB structure if the range of potential is fixed close to the first-neighbors distance (1nn). We have generalized the applicability of the potential by slightly modifying the parameters (see Table I and Fig. 1) and vanishing all interactions smoothly to zero just before the second-neighbor distance (2nn). The two body terms are plotted in Fig. 1 as a function of each interaction type. The new potential reproduces the

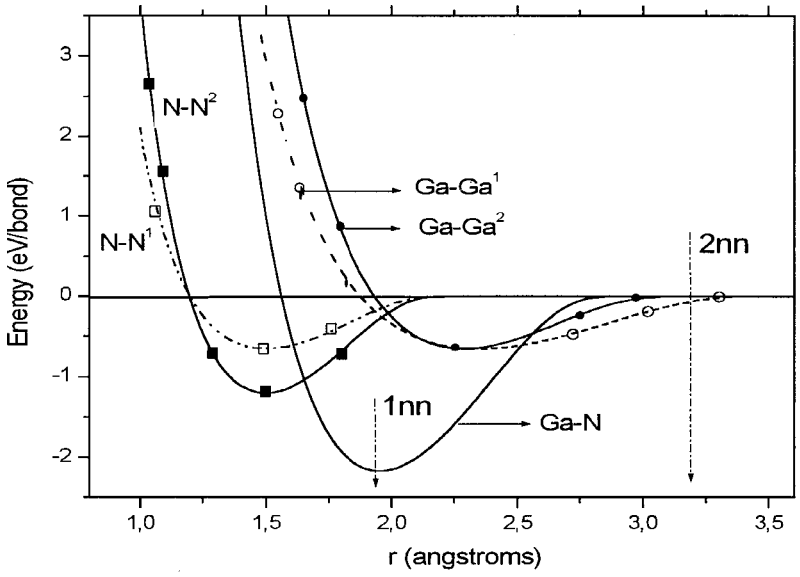

FIG. 1. Two-body terms as a function of each interaction type. The 1 and 2 digits refer to parameters given by Ref. 14 and the present work, respectively.

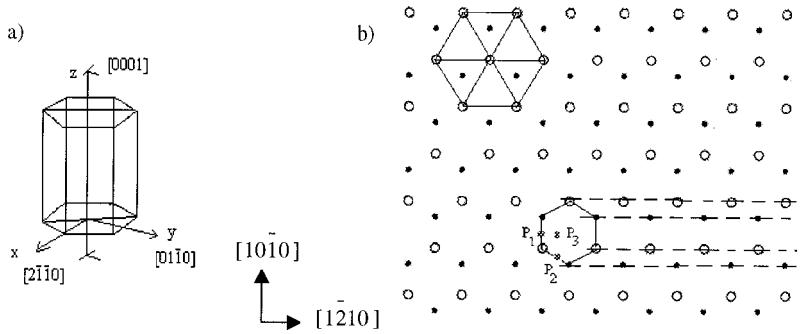

FIG. 2. (a) crystal geometry of the prism **a** edge dislocation. The dislocation lies along [0001] and glides on a $\{01\bar{1}0\}$ plane. (b) Projection into (0001) of the perfect crystal. The closed circles represent N atoms in *A* sites of the wurtzite lattice. The open circles represent Ga atoms in *B* sites. We notice that one closed circle superimposed one open circle and reciprocally. The points marked as P_1, P_2 and P_3 correspond to the origin for displacements when the dislocation is introduced.

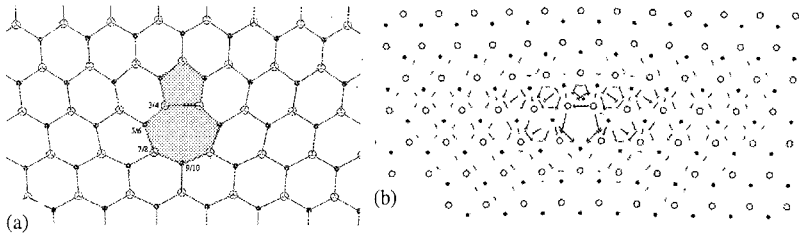

FIG. 3. Relaxed configuration of the **a** edge dislocation when the origin displacements is located in the point marked by P_2 in Fig. 2: (a) Core described by five- and seven-coordinated channels ($\frac{5}{7}$ core). It presents wrong bond (Ga-Ga) in this plane and (N-N) for the planes above and below. (b) Map of differential displacements of neighboring pairs of atoms.

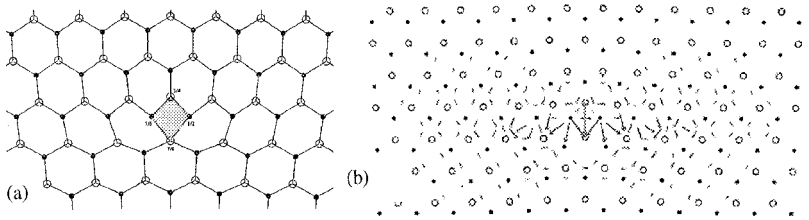

FIG. 4. Relaxed configuration of the **a** edge dislocation when the origin displacements is located in the point marked by P_1 in Fig. 2: (a) Core described by four-coordinated channels (four core). It is characterized by four bonds practically in the same plane. (b) Map of differential displacements of neighboring pairs of atoms.

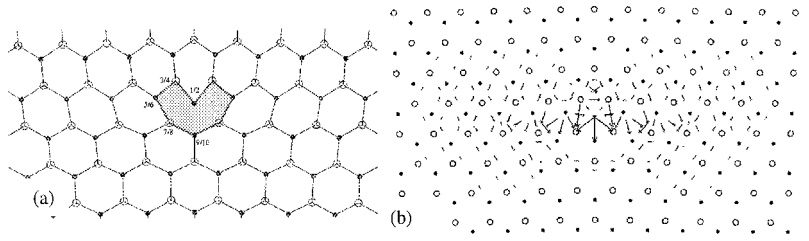

FIG. 5. Relaxed configuration of the **a** edge dislocation when the origin displacements is located in the point marked by P_3 in Fig. 2: (a) Core described by eight-coordinated channels (eight core). The core has a dangling bond. (b) Map of differential displacements of neighboring pairs of atoms.

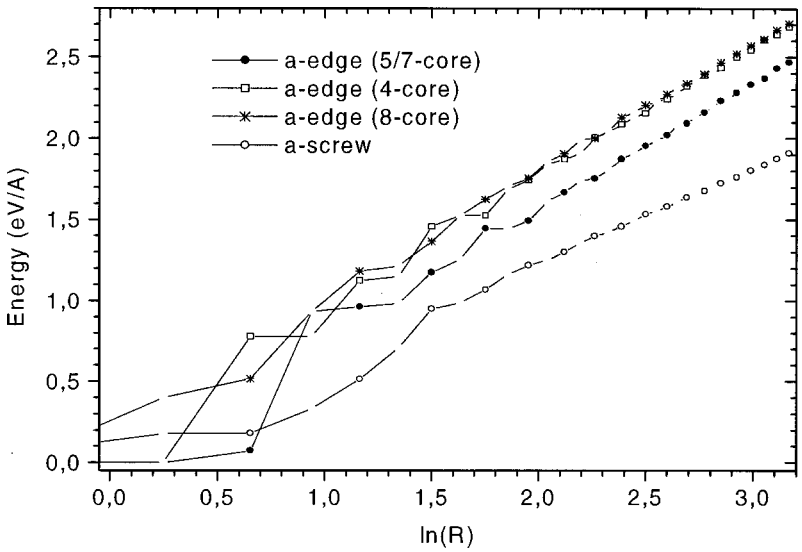

FIG. 6. Total energy stored in a cylinder of radius R as a function of $\ln(R)$ for the **a** dislocations.

lattice parameters and elastic constants; it stabilizes the IDB structure and reproduces the *ab initio* results[16] obtained for the length of the wrong bond crossing the boundary and the energy per unit area. The modified potential gives the IDB* as the most stable configuration although it overestimates its energy. In this work, we found that this potential is able to discriminate two close minima of similar energy corresponding to two configurations of the prism edge dislocation and gives results that may well compare with *ab initio* calculations as described below.

IV. CHARACTERIZATION OF THE DISLOCATION CORE

The strain energy of a dislocation within the linear elasticity theory, in an isotropic crystal is given by[7] $E = A_{th} \ln(R/r_c)$ where r_c is the dislocation core radius and R is the radius of a cylinder containing the dislocation line. The expression of the energy E does not include the core energy of the dislocations, where the linear elasticity theory cannot be applied.

The prelogarithmic factor A_{th} is $\mu b^2/4\pi(1-\nu)$ for the edge dislocation and $\mu b^2/4\pi$ for the screw, where b is the Burgers vector, μ is the shear modulus, and ν [0.37 for GaN (Ref. 18)] is the Poisson ratio. In Table II there are the expressions of the shear modulus as a function of the elastic constants and the prelogarithmic factors A_{th}^{SW} (from the elastic constants calculated with the potential) and A_{th}^{exp} (from the experimental elastic constants) for the edge and screw dislocations. The agreement between the two sets of values is consistent with the fact that the elastic constants are fitting parameters for the potential.

TABLE II. Expressions of the shear modulus μ as a function of the elastic constants C_{ij} (Ref. 7) and the theoretical prelogarithmic factors A_{th}^{SW} (eV/Å) and A_{th}^{exp} (eV/Å) for the edge and screw dislocations. The SW and experimental elastic constants are been reported in Ref. 14.

Defect	μ	A_{th}^{SW}	A_{th}^{exp}
Prism edge (**a**)	$(1-\nu)\dfrac{C_{11}^2-C_{12}^2}{2C_{11}}$	0.77	0.86
Basal screw (**a**)	$(C_{44}C_{66})^{1/2}$	0.56	0.58
Basal edge (**c**)	μ_B^e	2.16	2.24
Prism screw (**c**)	C_{44}	1.46	1.40

$$\mu_B^e=(1-\nu)(\sqrt{C_{11}C_{33}}+C_{13})\left(\frac{C_{44}(\sqrt{C_{11}C_{33}}-C_{13})}{C_{11}(\sqrt{C_{11}C_{33}}+C_{13}+2C_{44})}\right)^{1/2}$$

When the anisotropy of the crystal is considered, the prelogarithmic factor has to be substituted by the corresponding prelogarithmic factor A_0 of the energy of a straight dislocation of the same Burgers vector and line direction located in an anisotropic medium. This factor can be obtained either by applying the anisotropic elasticity theory[19] or directly by atomistic simulation[10,11,20,21] simulating the straight infinite dislocation and fitting the strain energy stored in the cylinder of radius R, containing the dislocation line, to the expression $E_s(R)=A_0 \ln(R/r_c)+E_c$, where E_c is the core energy.

Since the core energy is an integrated value it does not give information on the shape and extension of the dislocation core. This is better described by the map of differential displacements of neighboring pairs of atoms.[22] We apply both characterizations to analyze the dislocation cores.

V. DISLOCATIONS WITH $b=\frac{1}{3}\langle 11\bar{2}0\rangle$

A. Prism edge

This pure edge dislocation lies along [0001] and its glide plane is the $\{1\bar{1}00\}$ plane. The core presents three stable configurations that can be obtained by placing the dislocation line in the points marked as $P1$, $P2$, and $P3$, respectively, in Fig. 2. These points are the origins for the displacements imposed to the atoms to create the dislocation in the initial configuration before the relaxation. We can see that $P2$ is located between two closely spaced $(10\bar{1}0)$ planes whereas $P1$ and $P3$ are located between two widely spaced planes.

Figure 3(a) shows the relaxed core configuration of the dislocation with line dislocation origin located in $P2$. This

TABLE III. Minimum, maximum, and average bond lengths in Å around each site of *n*-coordinated channels of the **a** edge dislocation. In the *i*/*j* notation, a pair digital refers to Ga-atom site and an impair digital to N-atom site (see Figs. 3, 4, and 5). The equilibrium bond length is 1.96 Å.

n	work	1/2	3/4	5/6	7/8	9/10
8	Present	1.95-1.97 (1.96)	1.91-1.97 (1.94)	1.91-2.09 (1.97)	1.99-2.11 (2.06)	2.00-2.14 (2.07)
		1.97-1.97 (1.97)	1.91-1.95 (1.97)	1.91-2.07 (1.97)	1.99-2.14 (2.07)	2.00-2.11 (2.06)
	Elsner *et al.* (Ref. 26)	1.85-1.86 (1.85)	1.86-1.95 (1.91)	1.92-2.04 (1.97)	1.94-2.21 (2.06)	1.95-2.21 (2.11)
		1.88-1.89 (1.86)				
	Lee *et al.* (Ref. 23)	1.84±0.0	1.88±0.04	1.94±0.05	2.03±0.09	2.17±0.05
4	Present	1.94-2.29 (2.03)	1.92-1.93 (1.93)	1.94-2.30 (2.03)	1.99-2.25 (2.15)	
		1.93-2.25 (2.02)	1.92-1.94 (1.93)	1.93-2.25 (2.02)	1.99-2.30 (2.18)	
5/7	Present		1.92-2.26 (2.02)	1.96-2.02 (1.98)	1.08-2.08 (2.02)	1.99-2.08 (2.04)
			1.66-1.97 (1.89)	1.92-2.00 (1.97)	1.98-2.08 (2.02)	1.99-2.08 (2.04)
	Lee *et al.* (Ref. 23)		1.82±0.03	2.03±0.16	2.03±0.32	2.07±0.02

core presents a $\frac{5}{7}$-coordinated channel structure ($\frac{5}{7}$ core) with wrong bonds. Figure 3(b) shows the map of differential displacements of neighboring pairs of atoms[22] and demonstrates that the core is spread about $5a$ lattice parameters along the two adjacent $(10\bar{1}0)$ planes that contain the $\frac{5}{7}$-coordinated channel.

Figures 4(a) and 5(a) show the core structures of four- and eight-coordinated channel (four core and eight core) corresponding to the location of the line dislocation at $P1$ and $P3$, respectively. The four core is characterized by four bonds practically in the same plane and the eight core has a dangling bond. Figures 4(b) and 5(b) show that both structures have quite comparable displacement maps. The cores spread mainly in one $(10\bar{1}0)$ plane although displacements up to 5% of the Burgers vector length are distributed over the two adjacent planes in a region of about $7a$ lattice parameters. Potin and co-workers[2] presented HREM images of prism edge dislocations in GaN layers grown in a (0001) surface of sapphire. They report two possible core structures, namely, the four core and the eight core and claim that the $\frac{5}{7}$ core should be obtained by suppressing a row of atoms in the eight core. The same conclusion was obtained after density-functional (DF) tight-binding (TB) (Ref. 23) and *ab initio* simulations[24,25] and thus they refer to the $\frac{5}{7}$ core as an ''open'' core. Our results have shown that prism edge dislocations can be modelled simply by imposing the elastic displacements in a perfect crystal and allowing the system to relax without any further suppression or addition of atoms. The $\frac{5}{7}$ and the eight cores are related by a climb of the dislocation line.

Although the differential displacement maps give the shape of the dislocation core it is difficult to assign a core radius, i.e., the radius from where the elastic theory can be applied. Figure 6 shows the energy E_s stored in a cylinder of radius R as a function of $\ln(R)$ for the case of the **a** dislocation in a relaxable region of 46 Å of radius. For the $\frac{5}{7}$ core the slope is $A_0=0.78$ eV/Å and the curve starts being linear from $\ln(R/\text{Å})=1.9$ which gives a core radius of 6.7 Å and a core energy of 1.46 eV/Å. The obtained value of A_0 compares with the theoretical values given in Table II showing a coherency of the calculations, i.e., $A_0 \approx \mathbf{A}_{th}^{\mathrm{SW}}$, and validating the potential used since the discrepancy between A_0 and $\mathbf{A}_{th}^{\mathrm{exp}}$ is about 9%.

TABLE IV. Minimum, maximum, and average bond angles in degree around sites of *n*-coordinated channels of the **a** edge dislocation. In the *i*/*j* notation, a pair digital refers to Ga-atom site and an impair digital of N-atom site (see Figs. 3, 4, and 5). The equilibrium bond angle is 109.47°.

n	work	1/2	3/4	5/6	7/8	9/10
8	Present	94.2-108.4 (103.7)	90.9-119.7 (108.9)	93.7-131.2 (108.6)	86.6-127.4 (108.7)	104.9-124.8 (109.2)
		91.4-107.5 (102.1)	93.6-117.3 (109.3)	95.0-131.4 (108.9)	86.8-127.9 (108.7)	104.9-124.1 (109.1)
	Elsner *et al.* (Ref. 26)	112-118 (116)	97-119	100-129	94-125	100-122
		106-107				
	Lee *et al.* (Ref. 23)	108.5±0.6	105.4±4.1	107.0±17.6	110.8±15.9	110.4±8.6
4	Present	85.3-139.1 (107.6)	87.1-117.6 (109.3)	85.3-139.1 (107.5)	72.6-183.5 (104.1)	
		88.7-140.1 (108.3)	91.6-116.6 (109.3)	88.7-140.2 (108.3)	74.2-139.4 (104.0)	
5/7	Present		81.3-130.9 (107.7)	106.4-118.3 (109.5)	95.7-117.9 (109.0)	104.9-123.5 (109.2)
			98.7-137.6 (108.8)	97.8-121.2 (108.4)	98.6-117.3 (109.4)	104.4-124.0 (109.0)
	Lee *et al.* (Ref. 23)		114.7±0.2	106.9±13.3	109.1±12.0	110.2±8.0

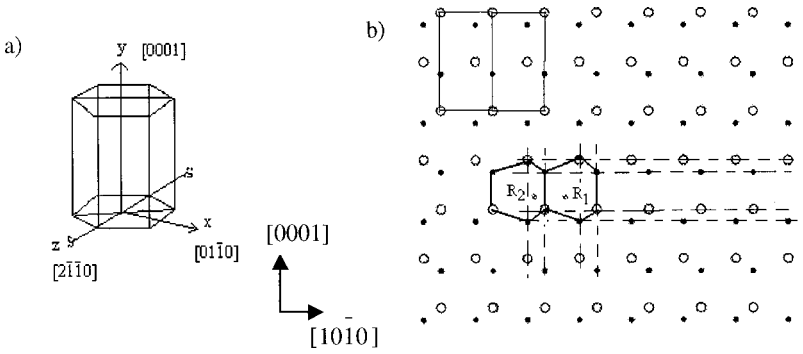

FIG. 7. (a) crystal geometry of the basal **a** screw dislocation. The dislocation lies along $\langle 2\bar{1}\bar{1}0\rangle$. (b) Projection along $[1\bar{2}10]$ of the perfect crystal. The closed circles represent N atoms in *A* sites (respectively, *B* sites) of the wurtzite lattice. The open circles represent Ga atoms in *B* sites (respectively, *A* sites). An h.c.p. unit cell is shown. The points marked as R_1 and R_2 correspond to the origin of displacements when the dislocation is introduced.

Similar studies of the total energy (E_s) against ln(R) have been done with the other two stable cores. The slope and the core radius for both configurations was found to be the same, as expected, than for the $\frac{5}{7}$ structure. However, the core energy ($Ec=1.72$ eV/Å) is 3% higher than that obtained for the $\frac{5}{7}$ structure core energy.

Tables III and IV describe the changes on the bond lengths and angles of the atoms that form the $\frac{5}{7}$, 8, and 4 coordinated channels and their first neighbors. The main distortion of these dislocation configurations is confined to $\pm 15\%$ for bond stretching and between -34% to $+28\%$ for bond bending. Bond lengths and angles with atoms at the $\frac{7}{8}$ and $\frac{9}{10}$ sites (see Figs. 3–5) for the $\frac{5}{7}$ and eight cores are consistent with previous calculations of the atomic displacements at the core.[23,26] According to our calculations the $\frac{5}{7}$ core is the most stable followed by the four and eight cores which cannot be discriminated since the difference in their energies is within the inaccuracy of the potential.

B. Basal screw

The dislocation core presents two stable configurations that can be obtained by placing the dislocation line in the points marked $R1$ and $R2$ in Fig. 7. As in the previous case, these points represent the origin of the displacements imposed to the atoms when the dislocation is introduced. We can see that $R2$ is located between two closely spaced $(10\bar{1}0)$ planes whereas $R1$ is located between two widely spaced planes. The displacement maps are presented in Fig. 8. In the two cases there are displacements in both basal and prism planes showing dislocation cores extended within a cylinder of a diameter of about $4a$ lattice parameters. The main difference between the two cores is in the displacements along the prism plane. The core $R2$ is located in one prism plane whereas the core $R1$ is distributed in two prism planes.

In Fig. 6, it is also shown the corresponding function of energy versus ln(R) calculated in a relaxable region of a radius of 46 Å for the $R2$ core. The slope is $A_0=0.59$ eV/Å and the curve starts being linear from $\ln(R)=1.9$ which gives a core radius of 6.7 Å and a core energy of 1.2 eV/Å. As in the edge case there is a good comparison between A_0 and the theoretical values (see Table II). The energy per unit length for the core $R1$ is 2% higher than the energy of the core $R2$.

VI. DISLOCATIONS WITH $b=[0001]$

A. Basal edge

The **c** edge dislocation has a $\{10\bar{1}0\}$ glide plane and lies along the $[1\bar{2}10]$ direction. The origins $S1$ and $S2$, chosen for the displacements of atoms when the dislocation is introduced are shown in Fig. 9. $S1$ is located between two widely spaced $(10\bar{1}0)$ planes. In this interplanar space each Ga atom of one plane is linked to one N atom of the other plane. $S2$ is located between two closely spaced $(10\bar{1}0)$ planes where each Ga atom of one plane is linked to two N atoms of the other plane.

The stable core configurations are shown in Figs. 10 and 11. The core shown in Fig. 10 has been obtained locating the dislocation line in the position $S1$. The map of relative displacements shows that the core is spread on two adjacent prism planes along a distance of 4 Burgers vectors. This core has lower energy than the core shown in Fig. 11 that has been obtained locating the dislocation line in the position $S2$. The map of relative displacements shows that the core is

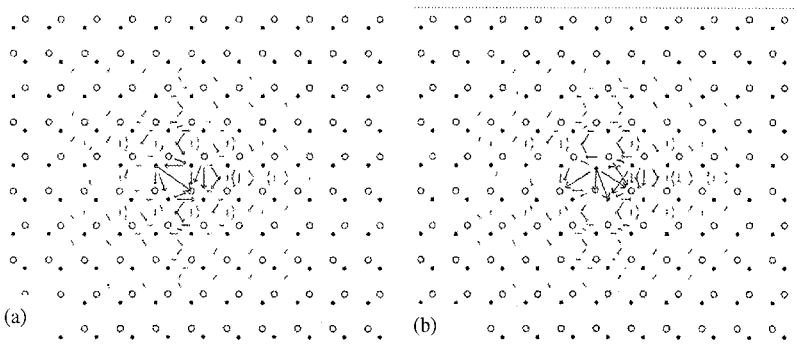

FIG. 8. Map of differential displacements of neighboring pairs of atoms of the relaxed core configurations of the **a** screw dislocation. The origin of displacements is located in R_2 (a) and in R_1 (b) according to Fig. 7.

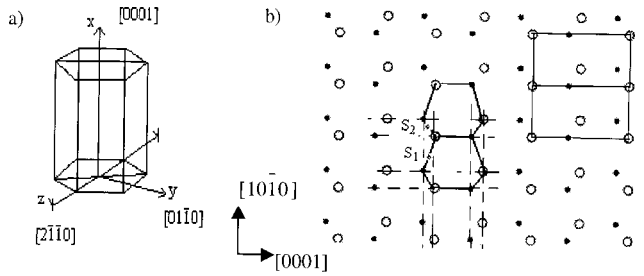

FIG. 9. (a) crystal geometry of the basal **c** edge dislocation. The dislocation lies along $\langle 2\bar{1}\bar{1}0\rangle$ and glides on a $\{01\bar{1}0\}$ plane. (b) Projection along $[1\bar{2}10]$ of the perfect crystal. The closed circles represent N atoms in *A* (respectively, *B*) sites of the wurtzite lattice. The open circles represent Ga atoms in *B* (respectively, *A*) sites. The origins of displacements when the dislocation is introduced are marked as S_1, S_2, S_3, and S_4.

extended to three prism planes and spread along 4 Burgers vectors. The slope of the strain energy for this dislocation is calculated to be 1.99 eV/Å that is about 8% smaller than the theoretical value. The core radius deduced for this configuration is 8.5 Å and its core energy 3.68 eV/Å (Fig. 12).

B. Prism screw

Figure 13 shows the location of the different origins of displacements studied ($T1$, $T2$, and $T3$) that led to the two dislocation cores reported. Positions $T1$ and $T2$ are equivalent.

The displacement map for the core obtained from $T1$ is presented in Fig. 14(a). The dislocation line in $T1$ is in a plane of mirror glide symmetry of the crystal and the displacements almost keep such symmetry. The map of relative displacements presents a core located inside a cylinder of radius $2a \approx 6.4$ Å. This configuration presents slightly smaller energy than $T3$. The second stable configuration $T3$ is obtained by relaxing the dislocation with dislocation line located in coincidence with the threefold axis of the crystal. The corresponding displacement map shows a core constrained into a cylinder of radius $1.5a \approx 4.8$ Å. We notice that the radius of the relaxable region where the dislocations were inserted was about 48 Å and thus, it can be considered that the influence of the fixed outer region in the relaxation of the core is negligible.

Figure 12 shows the corresponding function of energy versus $\ln(R)$ for the $T1$ core. The slope is $A_0 = 1.35$ eV/Å and the curve starts being linear from $\ln(R/\text{Å}) = 1.9$ which gives a core radius of 6.7 Å and a core energy of 2.82 eV/Å. As for the **c** edge dislocation, A_0 is 8% smaller than the theoretical value. The core radius, core energies and prelogarithmic factors of the studied dislocations are summarized in Table V.

VII. THE ACCURACY OF THE RESULTS: COMPARISON WITH *ab initio* CALCULATIONS

In this section we compare the energy calculations with some results reported in the literature obtained by *ab initio* methods (see Table V). We note that the *ab initio* results have been obtained in crystals of smaller sizes than in the present calculation. This implies that although the calculations are more precise the systems are often not fully relaxed. In order to compare the results we have calculated the energy of the dislocations within cylinders of the same radius as the ones used in the *ab initio* calculations.

Prism screw dislocation. Elsner and co-workers[25] report an energy of 4.88 eV/Å in a cylinder of radius 8.5 Å. Northrup[27] has simulated this dislocation using first-principles total energy calculations on a cylinder of a radius of 7.5 Å and he reports an energy per unit length of dislocation of 4.0 eV/Å. In the present simulation, when the total relaxable region has a radius of 46 Å, the energy inside a cylinder of 7.5 Å is about 2.9 eV/Å but if the relaxable region is constrained to the cylinder of a radius of 7.5 Å, then the energy is 3.3 eV/Å. The decrease of 0.4 eV/Å by increasing the size of the simulated crystal is directly related to the long-range relaxation that is not included in the 4.0 eV/Å given by Northrup. It seems reasonable to assign an error within the interval (0.3, 0.7) eV/Å to the core energy calculated in this work.

Prism edge dislocation. First principle calculations[24] performed with a supercell containing the eight-atom ring core gives an energy stored in a cylinder of radius equal to 8.5 Å of 2.19 eV/Å. The energy per unit length of this configuration for the same radius with the SW potential is 1.95 eV/Å. The difference of 0.24 eV/Å can be partly due to the bigger system (better relaxation) considered in the SW model. However, since this value is of the same order of the difference in energies for the $\frac{5}{7}$ core and eight core, it indicates that the SW model cannot discriminate which is the core of lower energy. In fact, Wright and Grossner[25] have calculated the formation energy of the $\frac{5}{7}$ and eight cores and have shown that they exhibit a pronounced dependence of the Fermi level. They report that the eight core has an energy lower than the $\frac{5}{7}$ core in the neutral charge state. However, recent DF-TB simulations[23] present the $\frac{5}{7}$-core structure as the most stable configuration in coincidence with our results.

Among the factors contributing to the inaccuracy of the

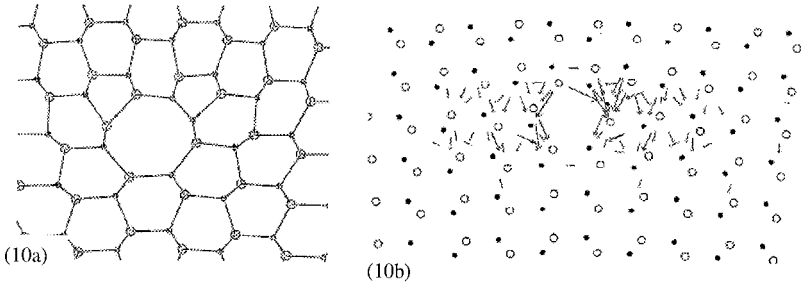

FIG. 10. (a) Core configurations and (b) map of differential displacements of neighboring pairs of atoms (b) of the **c** edge dislocation with origin of displacements in S_1 (see Fig. 9).

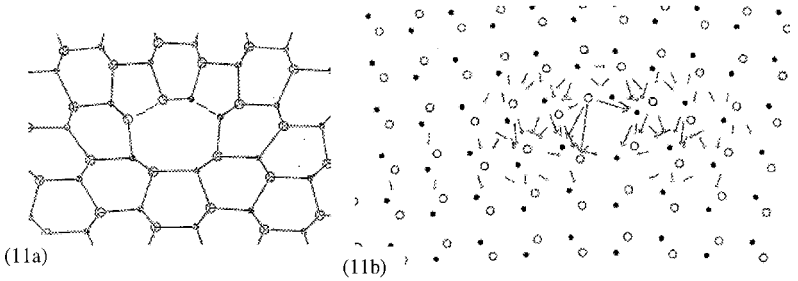

FIG. 11. (a) Core configurations and (b) map of differential displacements of neighboring pairs of atoms (b) of the **c** edge dislocation with origin of displacements in S_2 (see Fig. 9).

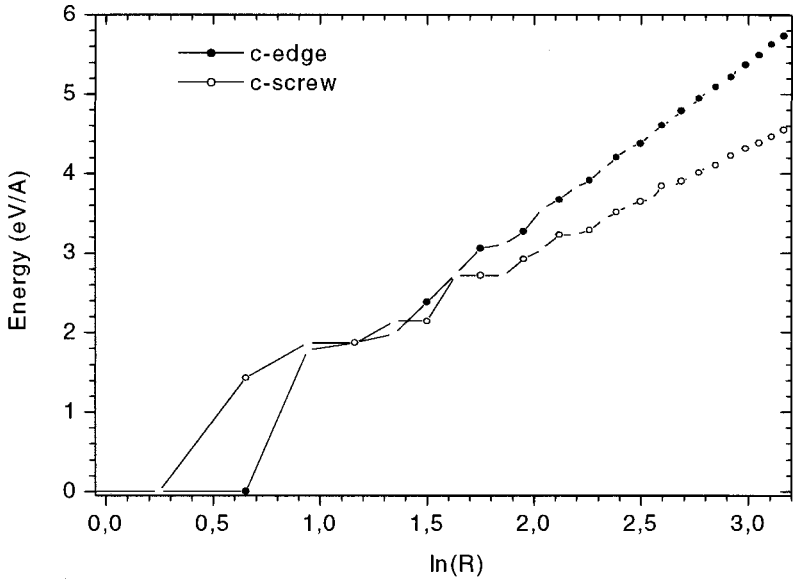

FIG. 12. Total energy stored in a cylinder of radius R as a function of $\ln(R)$ for the **c** dislocations.

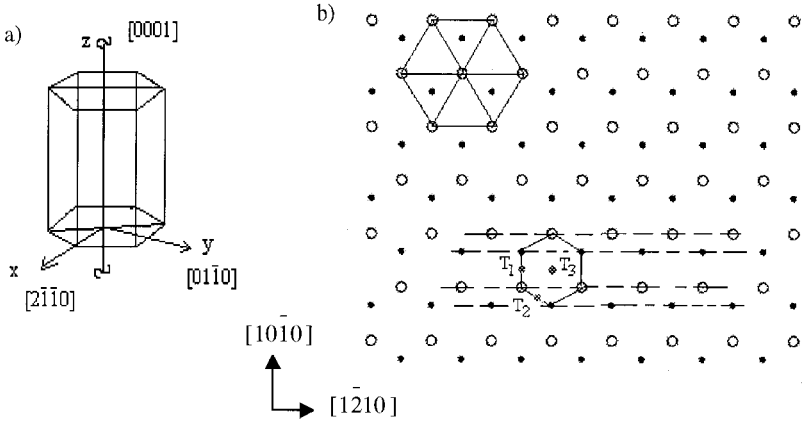

FIG. 13. (a) crystal geometry of the prism **c** screw dislocation. The dislocation lies along [0001]. (b) Projection into (0001) of the perfect crystal. The closed circles represent N atoms in A sites of the wurtzite lattice. The open circles represent Ga atoms in B sites. We notice that one closed circle superimposed one open circle and reciprocally. The points marked as T_1, T_2, and T_3 correspond to the origin for displacements when the dislocation is introduced.

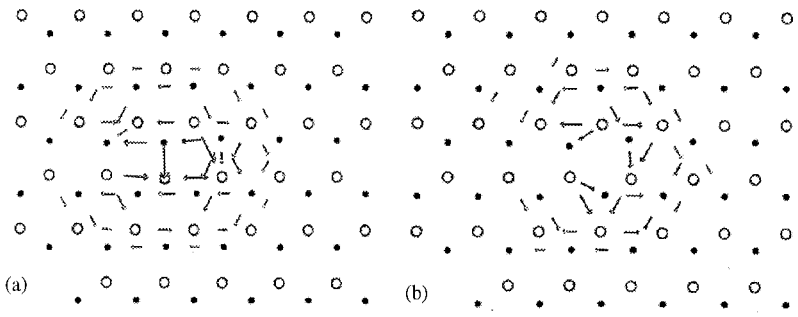

FIG. 14. Map of differential displacements of neighboring pairs of atoms of relaxed configurations of the **c** screw dislocation according to the origin of displacements in T_1 (a) and in T_3 (b).

TABLE V. Core radius (r_c), core energy (E_c), slope (A_0), and total energy obtained with the SW potential (E_T^{SW}) for dislocation structures. The total energy E_T^{FP} given by first-principles calculations is included for comparison.

Defect	Type Core	r_c (Å)	E_c (eV/Å)	A_0 (eV/Å)	E_T^{SW} (eV/Å) ($R=20$ Å)	E_T^{SW} (eV/Å)	E_T^{FP} (eV/Å)
	5/7	6.7	1.46	0.79	2.38		
Prism edge (**a**)	4	6.7	1.72	0.78	2.57		
	8	6.7	1.72	0.78	2.57	1.95[a] ($R=8.5$ Å)	2.19 (Ref. 24) ($R=8.5$ Å)
Basal screw (**a**)	$R2$	6.7	1.20	0.59	1.80		
Basal edge (**c**)	S_2	8.5	3.68	1.99	5.55		
Prism screw (**c**)	T_3	6.7	2.82	1.35	4.3	3.30[a] ($R=7.5$ Å)	4.00 (Ref. 27) ($R=7.5$ Å)
							4.88 (Ref. 24) ($A=8.5$ Å)

[a]The total relaxable region is constrained to the cylinder of radius R given in parentheses.

empirical potential there is the fact that such a potential cannot accurately describe radial and angular deformations simultaneously[28] and it does not consider explicitly the electronic effects. Moreover, being an empirical potential, it is affected by the experimental error assigned to the fitting parameters. Even though, the comparison with the *ab initio* results indicates that the SW potential gives a reasonable approximation of the energies and thus, SW is a suitable potential for the study of the stable atomic configurations of defects.

VIII. CONCLUDING REMARKS

We have simulated dislocations of both **a** and **c** Burgers vectors in a cylinder of a radius of 59 Å using an empirical potential of SW type. All dislocations have been generated by imposing the linear elastic displacement to a perfect crystal. The structure of the core depends on the location of the dislocation line. The stable atomic structures of the dislocation cores have been presented. The extension and shape of the dislocation cores have been analyzed by mapping the relative displacements of the atoms. The core radius and the core energy have been calculated by plotting the strain energy contained in a cylinder versus its radius.

We found three stable configurations for the prism **a** edge dislocation with structures described by $\frac{5}{7}$-coordinated channels, four- and eight-coordinated channels, respectively. The $\frac{5}{7}$ core presents, with the SW potential, the lowest energy. The four core, has similar energy as the eight core but different length and angles between bonds. The basal screw dislocation (*a* type) has two stable cores with a map of displacements extended within a cylinder of diameter about $4a_0$. It presents the main screw disregistry on the prism plane but there are important displacements distributed in the basal plane.

The **c** edge dislocation presents two stable configurations with cores spread along the glide plane with large displacements of the atoms. The **c** screw dislocation has two stable core configurations. These cores are quite homogeneously distributed around the dislocation line. These structures may favor the growing process and matches with the geometry of the open cores and nanotubes described in Ref. 6.

The difference between the prelogarithmic factors obtained from the linear elasticity theory (Table II) and by simulation (Table V) can be due to the anisotropy of the crystal. The core radius is calculated to be 6.7 Å for the *a*-type dislocation and *c*-screw dislocation and 8.5 Å for the *c*-edge dislocation. The core energy is deduced to be 1.46, 1.2, 3.68, and 2.82 eV/Å for the *a*-edge, *a*-screw, *c*-edge, and *c*-screw dislocations, respectively, with an accuracy of 0.3 eV/Å.

ACKNOWLEDGMENTS

The authors acknowledge the support of the UE (Contract No. HPRN-CT-1999-00040) and the Spanish MCYT (Grant No. BFM2000-0596-C03-03) and they are grateful to G. Nouet, P. Ruterana, and J. Chen for helpful discussions.

*Author to whom correspondence should be addressed. Electronic address: a.serra@upc.es

[1] A. Béré and A. Serra, Interface Sci. **9**, 149 (2001).
[2] V. Potin, P. Ruterana, G. Nouet, R. C. Pond, and H. Morkoç, Phys. Rev. B **61**, 5587 (2000).
[3] P. Vennégues, B. Beaumont, V. Bousquet, M. Vaille, and P. Gibart, J. Appl. Phys. **87**, 4175 (2000).
[4] Y. Xin, S. J. Pennycook, N. D. Browning, P. D. Nellist, S. Sivanathan, F. Ommnès, B. Neaumont, J. P. Faurie, and P. Gibart, Appl. Phys. Lett. **72**, 2680 (1998).
[5] W. Qian, G. S. Rohrer, M. Skoeronski, K. Doveerspike, L. B. Rowland, and D. K. Gaskill, Appl. Phys. Lett. **67**, 2284 (1995).
[6] P. Vennégues, B. Beaumont, M. Vaille, and P. Gibart, Appl. Phys. Lett. **70**, 2434 (1997).
[7] J. P. Hirth and J. Lothe, *Theory of Dislocations* (Wiley, New York, 1982).
[8] A. Serra and B. J. Bacon, Acta Metall. Mater. **43**, 4465 (1995).
[9] L. Verlet, Phys. Rev. **159**, 98 (1967).
[10] A. S. Nandedkar and J. Narayan, Philos. Mag. A **56**, 625 (1987).
[11] A. S. Nandedkar and J. Narayan, Philos. Mag. A **61**, 873 (1990).
[12] F. H. Stillinger and T. A. Weber, Phys. Rev. B **38**, 1537 (1985).
[13] M. Ichimura, Phys. Status Solidi A **153**, 431 (1996).
[14] N. Aïchoune, V. Potin, P. Ruterana, A. Hairie, G. Nouet, and E. Paumier, Comput. Mater. Sci. **17**, 380 (2000).

[15] D. B. Holt, J. Phys. Chem. Solids **30**, 1297 (1969).
[16] J. E. Northrup, J. Neugebauer, and L. T. Romano, Phys. Rev. Lett. **77**, 103 (1996).
[17] V. Potin, G. Nouet, and P. Ruterana, Appl. Phys. Lett. **74**, 947 (1999).
[18] V. A. Savastenko and A. U. Shelog, Phys. Status Solidi A **48**, K135 (1978).
[19] J. O. Schiffgens and K. E. Garrison, J. Appl. Phys. **43**, 3240 (1972).
[20] D. J. Bacon, D. M. Barnett, and R. O. Scattergood, Prog. Mater. Sci. **23**, 51 (1979).
[21] M. Heggie and M. Nylén, Philos. Mag. B **50**, 543 (1984).
[22] V. Vitek, R. C. Perrin, and D. K. Bowen, Philos. Mag. **21**, 1049 (1970).
[23] S. M. Lee, M. A. Belkhir, X. Y. Zhu, Y. H. Lee, Y. G. Hwang, and Th. Frauenheim, Phys. Rev. B **61**, 16 033 (2000).
[24] J. Elsner, R. Jones, P. K. Sitch, V. D. Porezag, M. Elstner, Th. Frauenheim, M. I. Heggie, S. Öberg, and P. R. Briddon, Phys. Rev. Lett. **79**, 3672 (1997).
[25] A. F. Wright and U. Grossner, Appl. Phys. Lett. **73**, 2751 (1998).
[26] J. Elsner, A. Th. Blumenau, Th. Frauenheim, R. Jones, and M. I. Heggie, MRS Internet J. Nitride Semicond. Res. **5S1**, W9.3 (2000).
[27] J. E. Northrup, Appl. Phys. Lett. **78**, 2288 (2001).
[28] B. Lebouvier, A. Hairie, F. Hairie, G. Nouet, and E. Paumier, Mater. Sci. Forum **207-209**, 277 (1996).